GEOLOGY

Near-universal trends in brGDGT lipid distributions in nature

Jonathan H. Raberg[1,2]*, Gifford H. Miller[1], Áslaug Geirsdóttir[2], Julio Sepúlveda[1]

Bacterial brGDGT lipids are a prevalent tool in studies of terrestrial paleoclimate. Their distributions correlate empirically with environmental temperature and pH, and their ubiquity in terrestrial, freshwater, and marine environments gives them wide applicability. Whether correlations with temperature and pH emerge due to a physiological response of source organisms and/or a shift in bacterial community composition remains an open question with important implications for proxy development and application. We applied a newly described technique for grouping brGDGTs to a globally compiled dataset ($n = 3129$) consisting of all modern sample media known to host brGDGTs. We found strong resemblances in the relationships between brGDGT fractional abundances and both temperature and pH across nearly all sample types examined. We also found near-universal connections between the brGDGTs themselves. Given the markedly different bacterial communities expected to inhabit these settings, these widespread relationships may suggest physiological and/or biochemical bases for observed brGDGT distributions.

INTRODUCTION

Lipid biomarkers preserved in sedimentary archives are an invaluable tool in studies of Earth's past climates. Of these, bacterial branched glycerol dialkyl glycerol tetraethers (brGDGTs) have quickly become one of the most popular proxies for reconstructing temperature and pH, partly because they are nearly ubiquitous in the natural world. BrGDGTs have been measured in more than a dozen of different sample media from the high Arctic (*1*) to the deepest ocean trenches (*2*), including in soil (*3*), peat (*4*), groundwater (*5*), hot springs (*6*), eolian particulate matter (*7*), marine hydrothermal (*8*) and methane cold seep (*9*) carbonate, fossil bone (*10*), speleothem (*11*), serpentinite-hosted ecosystems (*12*), and sediment and suspended/settling particulate matter (SPM) from lacustrine, riverine, and marine settings (*13*–*16*). This ubiquity, along with a preservation window of at least tens of millions of years (*17*), makes brGDGTs applicable in a wide variety of sedimentary archives over geologic time scales, even when other proxies may be absent (*18*–*23*). However, longstanding questions exist in brGDGT research that complicate their use as reliable, quantitative paleoclimate proxies.

The origin of the connection between brGDGT distributions and environmental parameters is one such pertinent question. Drawing analogies to other bacterial membrane lipid classes, early studies posited that the empirical relationships between brGDGTs and environmental parameters were physiological adaptations of source organisms to variations in external temperature and pH (*24*). Subsequent studies have since shown that changes in brGDGT distributions are also accompanied by shifts in the composition of the associated microbial community, indicating that the empirical correlations between the lipids and environmental parameters may be indirect in nature (*25*–*29*). Whether the variation in a brGDGT paleorecord is due to the direct physiological response of microbes to a changing environment or the indirect restructuring of a microbial community has important implications for its interpretation and fidelity (*28*). Unfortunately, brGDGT-producing source organisms remain incompletely identified and cultured (*30*), limiting our ability to test these hypotheses through controlled laboratory experimentation; to date, only two strains of Acidobacteria have been shown to produce just one of the 15 commonly measured brGDGTs (*31*, *32*). However, some insight can be gained by other means. Mesocosm studies of both incubated soils (*33*) and lake waters (*34*) have suggested a bacterial community influence. Molecular dynamics simulations have recently produced a split result, supporting the physiological explanation for the brGDGT paleothermometer but leaving open the possibility of a community-driven pH response (*35*). Here, we take an alternate approach in addressing this long-standing question by compiling the large and diverse body of existing lipid and environmental data and revisiting the empirical trends that exist in nature.

Early studies of brGDGTs in soils found that the number of methyl groups and cyclopentane rings on the lipids' alkyl backbone were empirically correlated with temperature and pH, respectively (*24*). Subsequent studies have generally upheld these basic relationships but have also found important differences in their details across sample types and regions. These discrepancies have led to independent modern calibrations for different sample types [e.g., soils and peats (*36*), lacustrine sediments (*37*) or SPM (*38*), bones (*39*), speleothems (*40*), and marine sediments (*23*)] and regions [e.g., East Africa (*41*) and China (*42*)] and have necessitated much effort to disentangle the allochthonous versus autochthonous sources of brGDGTs to sedimentary archives (*2*, *23*, *43*–*48*). Further complicating the matter, brGDGT distributions are affected by a wide array of other environmental parameters, including oxygen levels (*26*, *27*, *29*, *49*–*54*), salinity/electrical conductivity (*55*, *56*), seasonality (*27*, *36*, *46*, *57*), nutrient availability (*58*, *59*), and soil chemistry (*28*), which can mask or override relationships with temperature or pH. Last, an observed bias in brGDGT-derived temperatures toward warmer seasons has proven difficult to quantify, with various studies finding summer air temperature (*60*), the mean air temperature of months above freezing (MAF) (*36*, *37*, *55*), growing degree days above freezing (*61*), or other temperature indices to provide the strongest correlations in modern training sets. These discrepancies might be expected, as these air temperature indices are themselves only proxies for the in situ temperatures that are relevant for brGDGT-producing microbes. A growing body of in situ temperature studies [e.g., in lakes (*38*) and soils (*62*, *63*)]

[1]Department of Geological Sciences and Institute of Arctic and Alpine Research, University of Colorado Boulder, Boulder, CO 80309, USA. [2]Faculty of Earth Sciences, University of Iceland, Reykjavík, Iceland.
*Corresponding author. Email: jonathan.raberg@colorado.edu

show promise, but the vast majority of published works currently rely on air temperatures, which are more readily available.

BrGDGT studies have traditionally relied on fractional abundances (FAs) calculated by dividing the compound of interest by the sum of all 15 commonly measured brGDGTs ("Full Set FAs"; fig. S1G and table S1). By mathematically mixing these compounds in the denominator, this approach risks convoluting the influences of multiple environmental parameters on lipid distributions and obscuring individual compounds' trends. We recently proposed an alternative approach in which FAs are calculated within structurally based brGDGT subgroups (fig. S1 and table S1) (*55*). These "structural sets" deconvolved relationships among the lipids and temperature, pH, and conductivity in a global lake sediment dataset (*55*). Specifically, variations in methylation number, as isolated by the Meth Set (fig. S1A), captured the entirety of the brGDGT temperature response. Similarly, the pH response was fully captured by variations in cyclization number and isomer abundance, as quantified by the Cyclization-Isomer (Cyc-Isom) Set (fig. S1E). These clarified connections between lacustrine brGDGTs and their environment encourage application of the structural set approach to other sample types.

Here, we leverage the ubiquity of brGDGTs in nature and the clarifying capacity of the structural set methodology to determine whether evidence exists for a physiological basis underlying empirical temperature and pH trends. To this end, we compile a dataset (n = 3129) of all available modern sample media known to contain brGDGTs (Fig. 1 and table S2; see Materials and Methods). The wide range of sample types in the compiled dataset can be expected to host a correspondingly wide range of bacterial life (e.g., soil versus marine). If the relationships between brGDGTs and temperature/pH are physiological in origin, then they should supersede these taxonomic differences and produce similar trends across sample types. If, instead, bacterial community composition drives the link between brGDGTs and their environment, then different sample types should exhibit different environmental dependencies and coherent trends should not emerge. Here, we find that the structural set approach reveals relationships between brGDGTs and temperature and pH that are nearly universal across the diverse sample types in our compiled dataset. This result supports a physiological origin for the empirical connections between brGDGTs and their environment. We also find strong correlations [correlation coefficient (r) = 0.89] between pairs of brGDGT FAs and discuss their biochemical implications. Last, we note that, while physiology-driven trends emerge at a global scale, substantial variation persists at the regional or site-specific level, indicating that community composition and/or environmental factors outside of temperature and pH remain important controls on brGDGT distributions.

RESULTS

To determine whether evidence exists for a physiological brGDGT temperature response, we compared the relationships between brGDGT FAs and temperature across the sample types of the compiled dataset. These sample types do not always share the same temperature parameter [e.g., air temperature for soils versus sea surface temperature (SST) for marine sediments] due to inherent differences between sample types and data availability constraints (see Materials and Methods and Supplementary Text for details). However, trends can still be evaluated at the qualitative and semiquantitative levels to determine whether the brGDGT temperature response is similar across sample types.

The relationship between temperature and a representative compound, brGDGT-Ia, is shown in Fig. 2 for all sample types with associated temperatures in the compiled dataset. When the FA of brGDGT-Ia was calculated using all 15 commonly measured brGDGTs (Full Set; fIa_{Full}; Fig. 2A, fig. S1, and table S1), a weak correlation was observed across the dataset (r = 0.48; Fig. 2A), and linear fits of the six major sample types (soil, peat, lacustrine sediment, lacustrine SPM, marine sediment, and bone) varied widely in slope and intercept (Fig. 2B). However, when the FA of brGDGT-Ia was calculated in the Meth Set (fIa_{Meth}), which allows only methylation

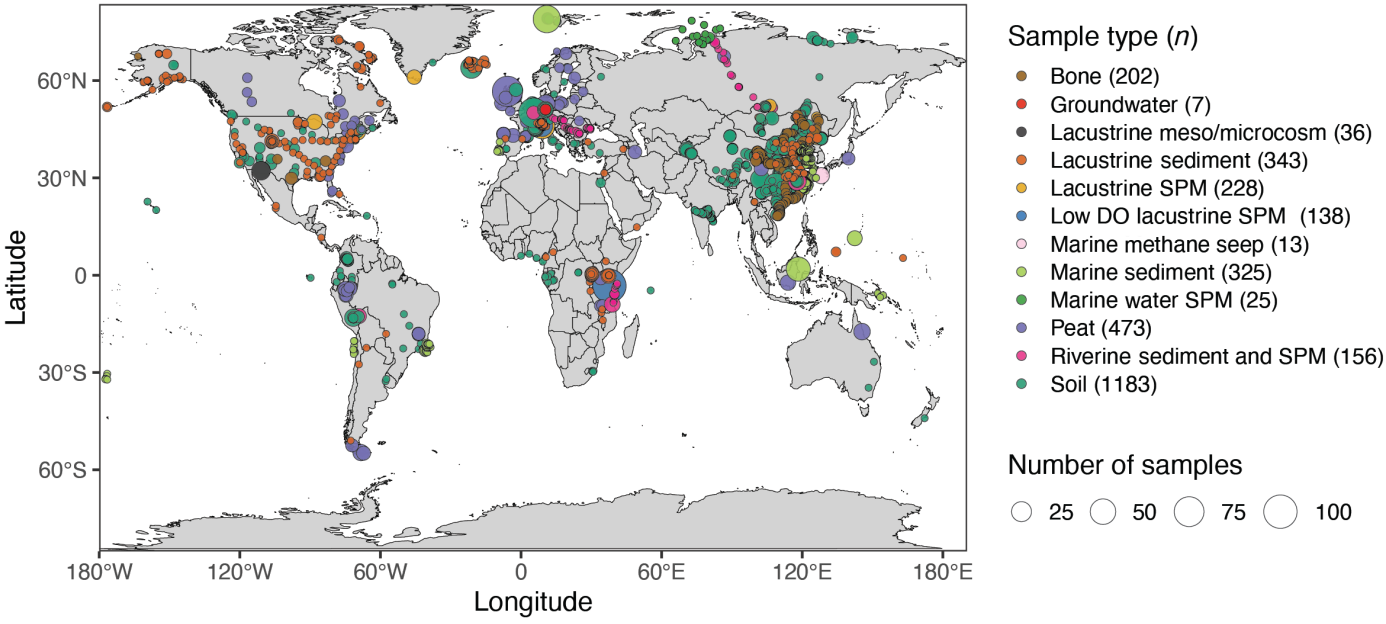

Fig. 1. Map of samples included in the compiled dataset. Number of samples (n) per sample type is given in the parentheses for a total of n = 3129.

number to vary by holding cyclization number and isomer designation constant (schematic at top right of Fig. 2, fig. S1, and table S1), a common temperature relationship emerged across sample types. The four sample types with existing global- or large-scale calibrations (soil, peat, lacustrine sediment, and bone) displayed similar functional forms with temperature, with linear slopes and intercepts often within uncertainty (Fig. 2D and fig. S2) and broad agreement overall (r = 0.79; Fig. 2C). Linear fits of marine sediments and lacustrine SPM, for which only smaller scale or site-specific calibrations have been generated (*23*, *38*), agreed with those of the major sample types (Fig. 2E), with fitting coefficients again often falling within uncertainty (Fig. 2F and fig. S2). Limited datasets of low dissolved oxygen (DO) lacustrine SPM (separated from other lacustrine SPM samples due to the marked influence of oxygen levels on brGDGT distributions), lacustrine meso/microcosm, and groundwater generally plotted within trends defined by the major sample types, resulting in a coherent temperature relationship across the dataset (r = 0.79; Fig. 2E).

The agreement in temperature trends across sample types was not limited to brGDGT-Ia. Rather, near-universal temperature trends were a common feature of the Meth Set (Fig. 3). The six major sample types again displayed visibly similar functional forms for all 15 compound FAs, with linear or quadratic fitting coefficients often falling within uncertainty (fig. S2). Notable deviations were visible for low DO SPM (e.g., Fig. 3E), groundwater (e.g., Fig. 3G), and marine samples (e.g., Fig. 3J) along with some soils and peats (e.g., Fig. 3A). As in Fig. 2, the Meth Set FAs unanimously provided stronger correlations than the standard Full Set FAs and better agreement across sample types (fig. S3).

To test the sensitivity of these results to our choice of temperature parameters, we repeated the above analysis using alternate associated temperatures for the four primary sample types (soil, peat, lacustrine sediment, and bone). When the same temperature parameter was used for all four sample types, the overall correlations and agreement between intercepts decreased slightly, while agreement between slopes was generally improved in comparison to the results in Fig. 3 (see Supplementary Text and a representative analysis in fig. S4).

To determine whether near-universal pH trends were also a feature of the compiled dataset, we examined the relationships between pH and brGDGT FAs calculated in the Cyc-Isom Set (fig. S1E and table S1). The Cyc-Isom Set, which holds the methylation number constant while allowing cyclization number and isomer designation to vary, was shown to best capture both the pH and conductivity dependencies of brGDGTs in lacustrine sediments (*55*). While pH is often measured in studies of brGDGTs, conductivity/salinity data are not widely available. We therefore compared trends in Cyc-Isom Set FAs with pH while noting that conductivity/salinity may additionally affect these FAs (e.g., for marine samples).

The relationships between Cyc-Isom brGDGT FAs and pH showed strong similarities across multiple sample types. Soils, peats, and lacustrine sediments and SPM exhibited compound-specific relationships with similar functional forms (Fig. 4) and linear slopes

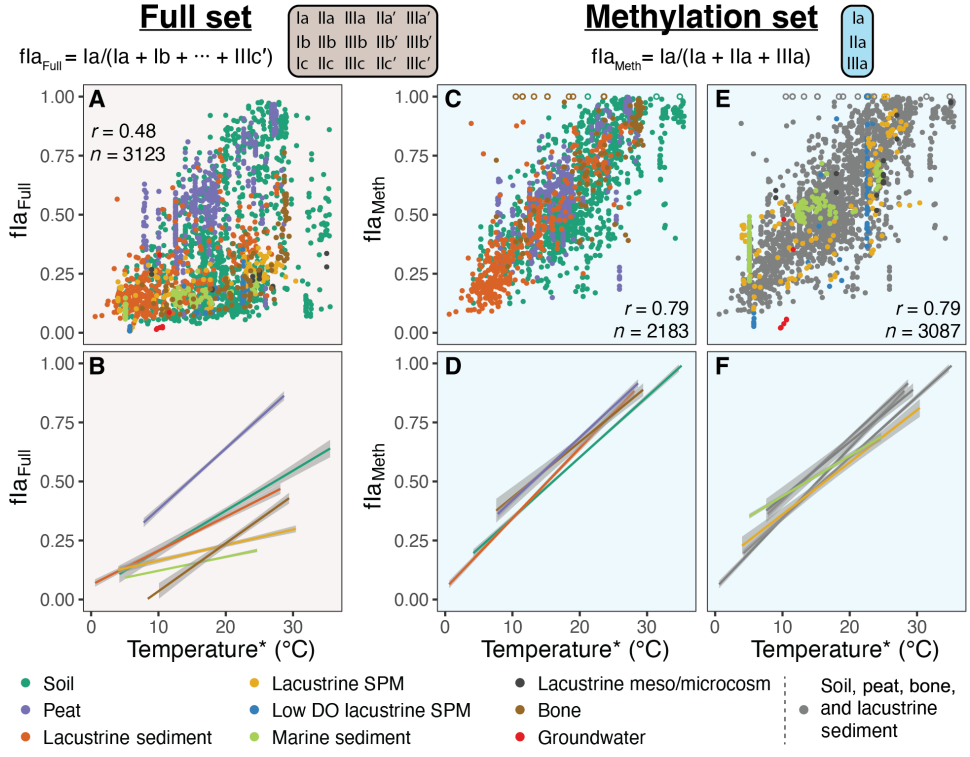

Fig. 2. Temperature trends across sample types for a representative compound, brGDGT-Ia. Relationship between temperature and the FA of brGDGT-Ia calculated in the (**A** and **B**) Full Set (fla$_{Full}$; schematic at top left; fig. S1G and table S1) and (**C** to **F**) Meth Set (fla$_{Meth}$; schematic at top right; fig. S1A and table S1). *Temperatures are (necessarily) different for different sample types (see Materials and Methods) and are as follows: warmest month air temperature (soil, peat, and bone), mean air temperature of months above freezing (lacustrine sediment), sea surface temperature (marine sediment), and in situ water temperature (SPM, meso/microcosm, and groundwater). Overall correlation coefficients (r) are provided for the n samples in (A), (C), and (E). Linear fits for the major sample types are plotted in (B), (D), and (F). Points and fits from (C) and (D) are plotted in gray in (E) and (F). $P < 0.01$ for all fits.

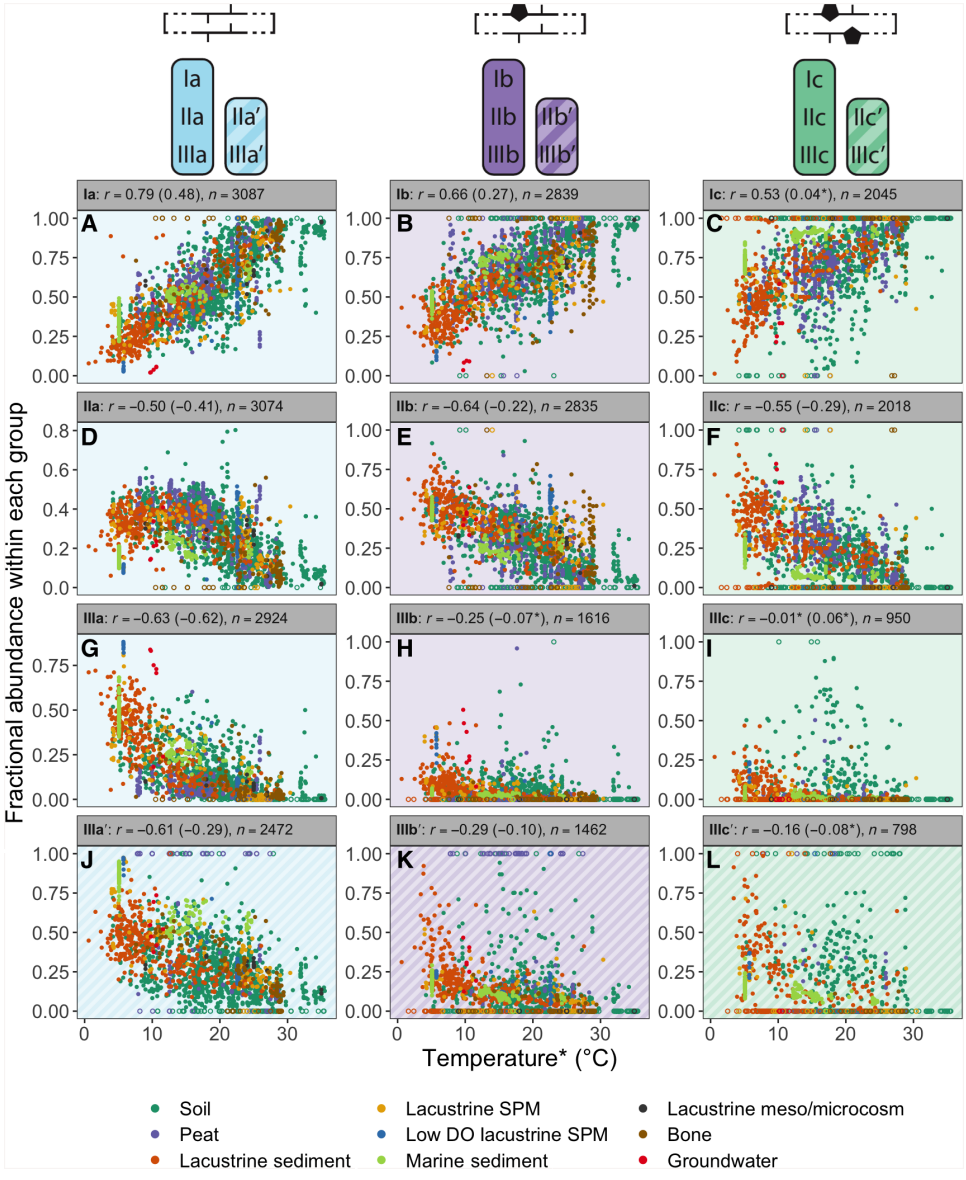

Fig. 3. Relationships between temperature and brGDGT FAs for each compound (A to L) in the Meth Set. The Meth Set is formed by grouping brGDGTs by cyclization number and isomer designation (schematics at top); FAs are calculated within each group (*55*). Plots of IIa′, IIb′, and IIc′ exactly mirror those of IIIa′, IIIb′, and IIIc′, respectively, and are therefore not shown. *Temperatures are the same as in Fig. 2. Correlation coefficients (*r*; quadratic for IIa and IIIa and linear for all other compounds) are provided for each Meth Set FA, with coefficients for the corresponding Full Set FA (calculated using all 15 compounds) given in parentheses for comparison. $P < 0.01$ except where marked with an asterisk. Open circles denote points with FA = 0 or 1. These points were primarily clear outliers originating from samples with low concentrations of brGDGTs and were excluded from statistical analyses (see Materials and Methods).

often within 1 SE (fig. S5). However, unlike for temperature, a consistent offset is visible between the terrestrial (soil and peat) and lacustrine (sediment and SPM) datasets (Fig. 4). Sample types with limited datasets—including lacustrine meso/microcosm and low DO SPM, riverine sediments and SPM, marine sediments, and groundwater—generally plot within these global trends, with notable exceptions for low DO SPM, marine sediments, and groundwater samples (e.g., Fig. 4E). Lower pH microcosm samples also deviated, potentially due to the death of brGDGT-producing microbes in these experiments (*34*), and riverine sediments from an acid mine drainage (*64*) were consistent outliers. Again, the Cyc-Isom FAs provided stronger correlations and better agreement between sample types than the standard Full Set approach (fig. S6).

In addition to the structural sets, multiple indices have been developed to highlight brGDGT structural variations. Three of the most widely applied are MBT'_{5Me} (*65*), CBT′ (*65*), and IR_{6Me} (*66*), which highlight changes in methylation number, cyclization number, and isomer abundance, respectively. Coherencies in the relationships between all three indices and temperature or pH were present across sample types (Fig. 5, A to C), with correlation coefficients as high as $r = -0.85$. In addition, linear regressions between MBT'_{5Me} and temperature were in broad agreement for the six major sample

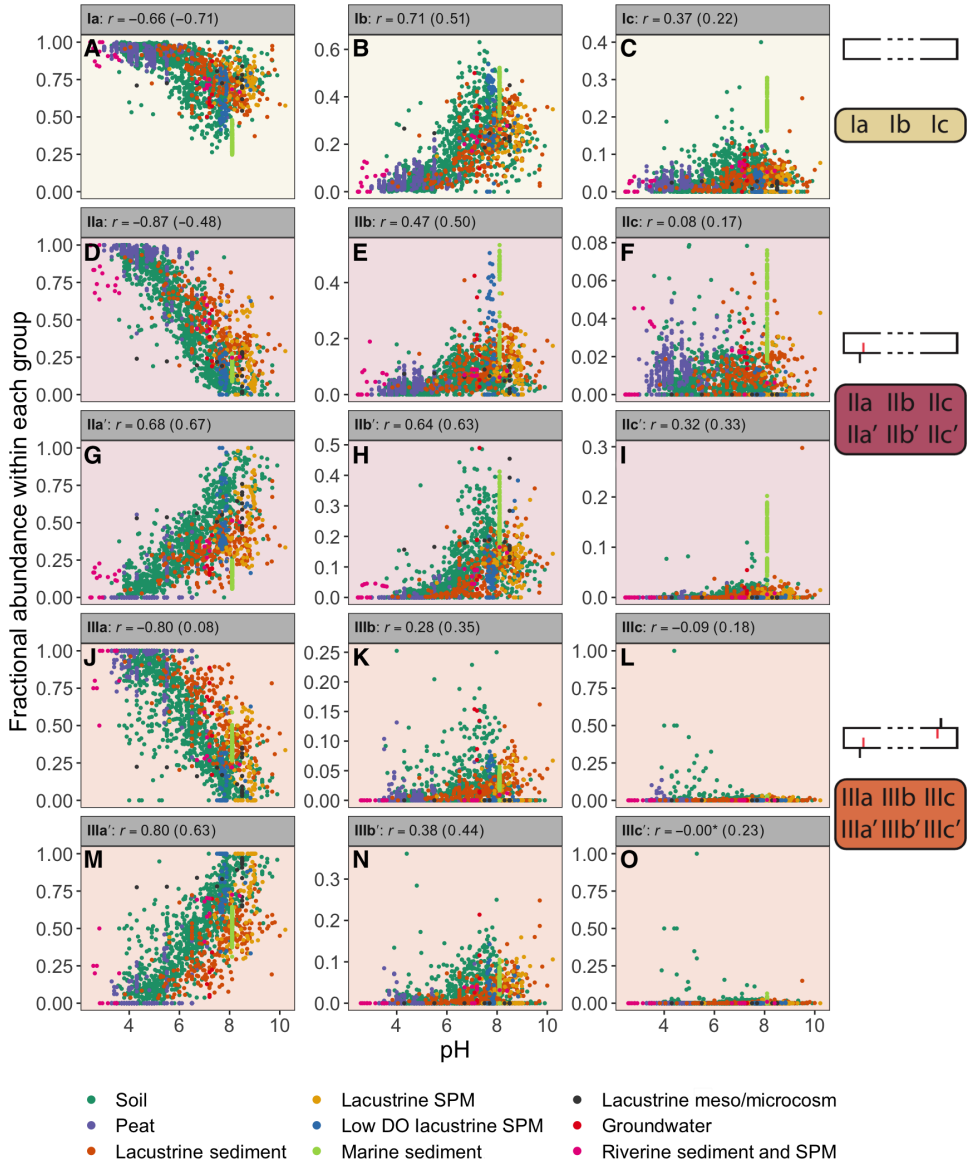

Fig. 4. Relationships between pH and brGDGT FAs for each compound (A to O) calculated within the Cyc-Isom Set. The Cyc-Isom Set is formed by grouping brGDGTs by methylation number [schematics at right and methylations at C5 (black) or C6 (red)]; FAs are calculated within each group (*55*). Linear correlation coefficients (*r*) are provided for each Cyc-Isom Set FA, with coefficients for the corresponding Full Set FA (calculated using all 15 compounds) given in parentheses for comparison. $P < 0.01$ except where marked with an asterisk. $N = 1864$ for all subplots.

types (Fig. 5D). Regressions of the pH indices, CBT′ and IR_{6Me}, displayed larger differences (Fig. 5, E and F), although we note that most of these sample types do not span the full range of pH values. Last, we note that the structural set analyses (Figs. 3 and 4) suggest that the common trends in these widely applied indices originate from coherencies at the compound-specific level.

In addition to correlations with temperature and pH, we found multiple near-universal relationships between pairs of brGDGT FAs (Fig. 6). By partitioning brGDGTs into the structural sets, these pairs of FAs are guaranteed to be mathematically independent (*55*). The FAs of uncyclized and monocyclized tetramethylated brGDGTs (fIa_{MI} and fIb_{MI}; fig. S1D and table S1) were tightly correlated in the Meth-Isom Set ($r = 0.89$; Fig. 6A). Similarly, those of 5-methyl pentamethylated and hexamethylated uncyclized brGDGTs ($fIIa_{CI}$ and $fIIIa_{CI}$; fig. S1E and table S1) were closely related in the Cyc-Isom Set ($r = 0.89$, Fig. 6B). Last, 6-methyl isomers of pentamethylated and hexamethylated uncyclized brGDGTs ($fIIa'_{Isom}$ and $fIIIa'_{Isom}$; fig. S1C and table S1) were present in proportional abundances in the Isom Set ($r = 0.89$; Fig. 6C). These relationships were broadly consistent across sample types, with linear slopes and intercepts often within error (fig. S7). A comparable analysis is not possible using traditional Full Set FAs, as they are not mathematically independent (all compounds appear in the denominator).

While the basic functional forms of the relationships among brGDGTs, temperature, and pH are in good agreement, differences may be present in their details. An analysis of the fitting coefficients for each sample type revealed that they are often but not always within 1 SE. However, challenges, such as a lack of standardized

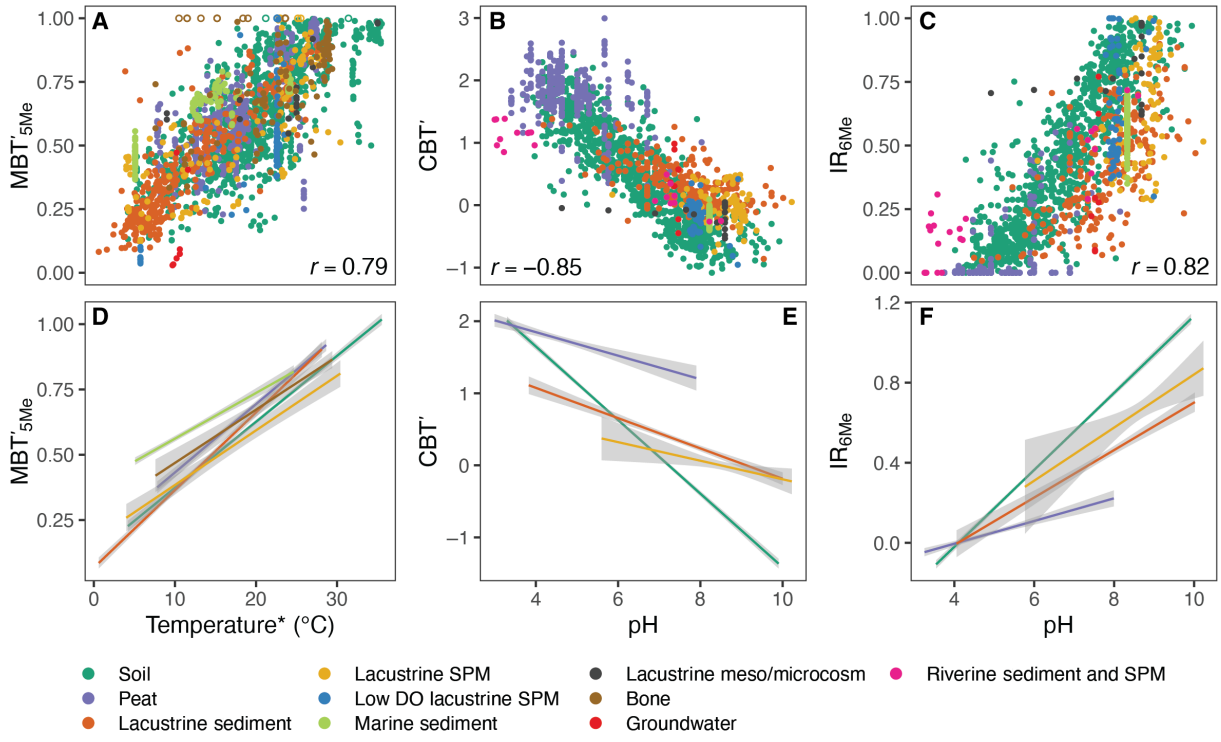

Fig. 5. Relationships between common brGDGT indices and temperature or pH. *Temperatures are the same as in Fig. 2. Overall correlation coefficients (*r*) are provided for (**A**) to (**C**). Linear fits for each of the major sample types are plotted in (**D**) to (**F**). $P < 0.01$ for all fits except that of pH and CBT′ for lacustrine SPM, for which $P = 0.013$.

temperature measurements between sample types, limit the utility of this approach at this point. An expanded discussion of these challenges is available in Supplementary Text.

DISCUSSION

Microbial community composition can be expected to vary markedly across the diverse media and environments of the compiled dataset. The fact that near-universal temperature and pH trends supersede these community differences is therefore remarkable and suggests that either (i) brGDGTs are produced by a small number of widespread source organisms or (ii) brGDGTs play a fundamental physiological role for a wide range of bacterial life. In either case, these near-universal trends have important implications for brGDGT-based proxies. First, they encourage proxy development beyond the well-studied soil/peat and lake sediment datasets. In particular, they support recent work in marine sediments (*23*, *67*, *68*), which exhibited the highest compound-specific temperature correlation in our dataset (fIa_{Meth}; $r = 0.88$), as well as in bones (*39*) and lacustrine SPM (*38*). The widespread trends also suggest that it may be possible to construct modern calibrations that join multiple sample types in future studies. Currently, the sample types in the compiled dataset (necessarily) have different associated temperatures (e.g., air versus water; see Materials and Methods) and exhibit offsets in pH relationships (Fig. 4 and fig. S5). While these incongruities preclude the construction of universal calibrations at this time, advances in brGDGT research, such as the growing body of in situ (*62*, *63*) and/or more standardizable (*69*) temperature measurements, may allow for such efforts to succeed in the future. Even without these mixed or universal calibrations, the common functional forms exhibited by different sample types lend confidence to qualitative trends in paleoclimate reconstructions from mixed-source archives (provided that the relative contribution of each source can be constrained). Furthermore, the commonalities in brGDGT temperature and pH responses support the use of the proxies in paleoclimate reconstructions where modern analogs and details of the depositional setting may be unavailable (e.g., deep time settings).

Correlations between pairs of brGDGT FAs (Fig. 6) revealed relationships between lipids that spanned nearly every sample type examined. Such connections may provide insight into the biosynthesis and/or biochemical roles of brGDGTs in cells. For example, the correlated Isom Set FAs of IIa′ and IIIa′ (Fig. 6C) may indicate that the same enzyme is responsible for methylating both compounds and/or that the two lipids perform related functions. Similarly, Fig. 6A revealed that if the most abundant uncyclized compound is Ia (high fIa_{MI}), then the most abundant monocyclized compound will be Ib (high fIb_{MI}). This link may suggest that (i) the enzyme responsible for altering the methylation number is able to do so regardless of the presence of a cyclopentane ring, (ii) the ring is formed after methylation number has already been set, or (iii) the two compounds perform a related function for the cell that is independent of ring number. New avenues of research based on such observations may provide rare insight into the biochemistry of brGDGTs.

Deviations from the trends described above are nearly as important as the trends themselves. Samples with low associated DO, such as groundwater and some lacustrine SPM, show anomalously high $fIIIa_{Meth}$ (Fig. 3G), which would lead to underestimates of temperature using most brGDGT transfer functions. These samples are also

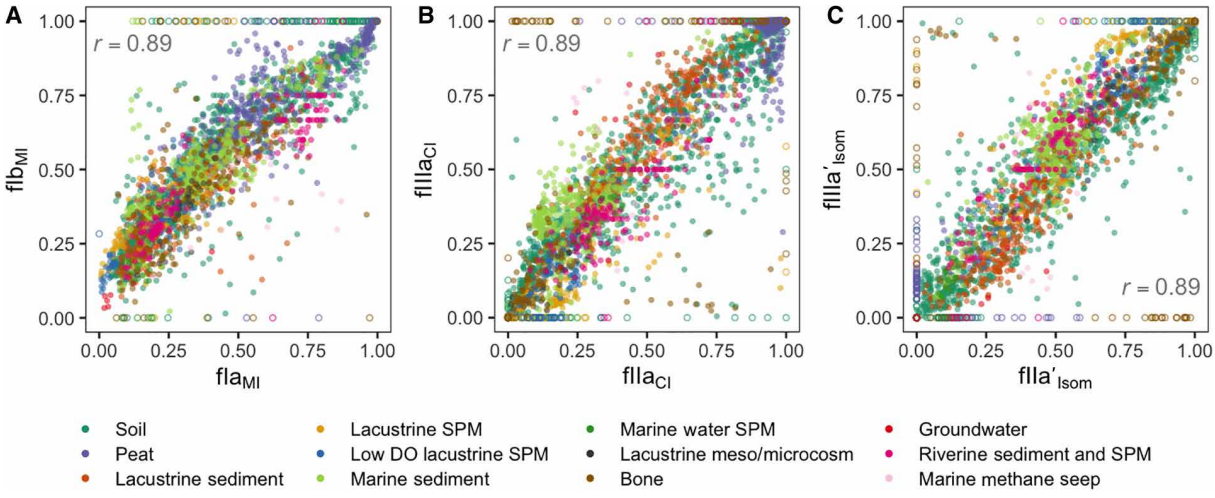

Fig. 6. Relationships between selected brGDGT FAs. FAs were calculated in the (**A**) Meth-Isom (MI), (**B**) Cyc-Isom (CI), and (**C**) Isom structural sets (fig. S1 and table S1) (*55*). Correlation coefficients (*r*) for linear regressions are provided ($P < 0.01$ for all). Samples with FA = 1 or 0 (open circles) were excluded from statistical analyses [$n = 2908$, 2557, and 2348 for (A) to (C), respectively]. FAs are calculated as follows (fig. S1 and table S1): fla_{MI} = Ia/(Ia + IIa + IIIa + IIa′ + IIIa′) and flb_{MI} = Ib/(Ib + IIb + IIIb + IIb′ + IIIb′); $flla_{CI}$ = IIa/(IIa + IIb + IIc + IIa′ + IIb′ + IIc′) and $fllla_{CI}$ = IIIa/(IIIa + IIIb + IIIc + IIIa′ + IIIb′ + IIIc′); and $flla'_{Isom}$ = IIa′/(IIa + IIa′) and $fllla'_{Isom}$ = IIIa′/(IIIa + IIIa′).

associated with narrow pH ranges yet vary widely in cyclization and isomer abundances (e.g., Fig. 4E), indicating an unconstrained influence of bacterial community composition, source mixing, or environmental variables outside of temperature and pH. In addition, the origin of the offset between the pH responses of terrestrial and lacustrine samples (e.g., Fig. 4J) is unknown. While it is possible that this discrepancy represents important differences between these sample media, it is also possible that bulk pH measurements do not accurately represent the chemical microenvironments experienced by brGDGT-producing microbes (e.g., in soils) (*70*). These or other possibilities warrant further investigation. Last, we stress that, while clear trends emerge at the global scale, they do not always hold at the regional or site-specific level [e.g., (*27*)], indicating that microbial community effects and/or environmental forcing outside of temperature and pH remain as important controls.

Examination of a given sample in the context of the compiled dataset may serve as a tool for evaluating brGDGT sources, identifying uncommon distributions, or determining when other environmental parameters may be at play. For example, riverine sediment from an acid mine drainage with water pH of ~2.9 deviated from broader pH trends (Fig. 4). This deviation may indicate uncommon patterns of brGDGT production driven by extreme environmental conditions (*64*). However, it may also suggest that a substantial percentage of these brGDGTs are derived from the surrounding soils, whose higher average pH of ~4.2 would place them in better agreement with global trends. Marine sediments also showed multiple anomalous relationships with pH (e.g., Fig. 4E). Many of these samples are from coastal margins near major freshwater outflows, however, where water chemistry (e.g., salinity, pH, and nutrients) can vary widely with depth and season [e.g., Svalbard fjords (*71*) and references within]. Their incongruity thus highlights an opportunity to link marine brGDGT production to time- and depth-variant environmental conditions and/or bacterial community compositions. It may also indicate the need to include brGDGTs beyond the set of 15 commonly measured compounds, such as the salinity-linked 7-methyl isomers (*55*, *56*). Last, relationships between pairs of brGDGT FAs (Fig. 6) may provide a useful tool for highlighting unusual brGDGT distributions. An outlier from these trends would display a brGDGT composition that is unique across nearly 3000 samples from one dozen globally distributed sample types. Such outliers could point to uncommon brGDGT distributions, functions, or producers in both modern and ancient samples.

In conclusion, a comparison of 3129 samples spanning one dozen sample types from across the globe revealed near-universal trends among brGDGTs, temperature, and pH. Ten distinct relationships displayed *r* values with magnitudes between 0.79 and 0.89 across 8 to 12 diverse sample media (Figs. 3A; 4, D, J, and M; 5, A to C; and 6, A to C). Other relationships exhibited weaker, yet significant, correlations but still had similar functional forms (e.g., Fig. 3D). Recent work has revealed that brGDGT distributions vary in tandem with bacterial communities (*25*–*29*, *34*), connecting them only indirectly to pertinent variables such as temperature and pH. However, given the wide range of microbial life expected to inhabit the diverse environments of the compiled dataset, the coherent trends presented here suggest at least some physiological basis for the relationships between brGDGTs and their environment. This observation encourages the further development of brGDGT-based proxies, lends confidence to their continued application, and provides a new framework for investigating controls on brGDGT distributions in the future.

MATERIALS AND METHODS

Experimental design

The objective of this study was to compare how brGDGTs in different sample types relate to temperature, pH, and one another. While brGDGT FAs can be quantitatively compared without trouble, environmental parameters pose a challenge. First, temperatures associated with different sample types are often different (e.g., air versus water temperature), with seasonality effects further complicating temperature selection (e.g., summer versus mean annual). Furthermore, many commonly used measurements are themselves only proxies for the true environmental conditions experienced by brGDGT-producing

microbes. For example, air temperature is commonly used in place of in situ soil temperature, although the annual means of the two can differ by as much as 10°C (*72*). As a result, it is not possible at this time to standardize environmental parameters, such that datasets of different sample types can be fully quantitatively merged. However, qualitative and semiquantitative comparisons of the ways in which brGDGTs relate to temperature and pH can still provide meaningful results with important implications and are worthy of pursuit.

To this end, we compiled the brGDGT FAs and, to the best of our ability, associated temperature and pH values from previously published datasets. We selected temperature parameters that were widely supported in the literature when possible. Where a consensus had yet to be reached (e.g., marine sediments), we selected standardizable and accessible parameters (e.g., SSTs). These selections are not intended to opine on these areas of research, only to allow for broad comparison with other sample types in this study, and they could be further explored in future studies.

Sample types and associated environmental parameters

Lipid and environmental data were compiled from previously published datasets of modern samples that used the most recent chromatographic methods that separate 5- and 6-methyl isomers (*65*). The compiled dataset (n = 3129; Fig. 1 and table S2) consisted of bone (n = 202), groundwater (n = 7), lake water meso/microcosm (n = 36), lake surface sediment (n = 343), lake water SPM [n = 228; including sediment traps (n = 115) and water filtrates (n = 113)], low DO lake water SPM [n = 138; including sediment traps (n = 29) and water filtrates (n = 109)], authigenic carbonates from a marine methane cold seep (n = 13), marine surface sediment [n = 325; including deep ocean trench sediments (n = 31)], marine SPM (water filtrates, n = 25), peat (n = 473), riverine surface sediments (n = 71) and SPM (n = 85; water filtrates), and soil [n = 1183; including permafrost active layer (n = 17)]. Data from other sample media—including hot springs, speleothems, and hydrothermal vents—could not be included, as these studies did not separate the 5- and 6-methyl isomers. All data and references are available in data file S1 and in (*73*). FAs were calculated according to fig. S1 and table S1 [see (*55*) for further details].

Temperatures associated with each sample type are as follows: mean air temperature of months above freezing (MAF; lacustrine surface sediments), warmest month temperature (WMT; soils, peats, and bones), in situ water temperature [lacustrine SPM (integrated summer water column where available for sediment traps, point measurement otherwise), meso/microcosm, and groundwater], SST of the warmest month (marine sediments above 72°N), and mean annual SST (all other marine sediments). These temperatures were primarily based on previous calibrations and data availability, with some adjustments as follows.

Lacustrine sediments have recently been shown to correlate with the MAF warm season air temperature index on a global scale (*37*, *55*). Soil and peat brGDGTs have also been shown to correlate with MAF (*36*). However, we used another warm season temperature index, WMT, which provided comparable compound-specific correlations and better overlap with other sample types in this study (see Supplementary Text and fig. S4). Where these temperature parameters were not published, we generated monthly air temperature normals (1970–2000) using the WorldClim database (*74*).

Although bones were initially calibrated against mean annual air temperature, a warm season bias was observed in that study (*39*). Because of this bias and to match the soil and peat datasets, we used WMT values generated with the WorldClim database as above. Only bones with substantial in situ brGDGT production (isomer ratio >50%) were included in temperature analyses (*39*).

Temperature calibrations for brGDGTs in marine settings are an active area of research. Thus far, brGDGT production has been demonstrated in both deep (*54*) and shallow (*75*) marine water columns, and correlations have been found between marine surface sediment brGDGTs and both sea surface (*67*, *68*) and bottom water (*23*) temperatures. Because of these uncertainties and data availability constraints, we used the SST parameter for marine sediments in this study. Where published data were not available, we generated SSTs using the Extended Reconstructed Sea Surface Temperature database (*76*). We used mean annual SST except for the northernmost sites (>72°N), which experience substantial sea ice cover, for which we used the SST of the warmest month. To avoid marine sediments with terrestrial influence, we excluded those samples with a $\#rings_{tetra}$ (*48*) index < 0.7 or (IIIa + IIIa′)/(IIa + IIa′) < 0.92 from temperature analyses (*2*, *68*).

A calibration has yet to be generated for lake water filtrates; however, point measurements of water temperature taken at the time of sampling are widely available and were thus used in this study. Integrated summer (June, July, and August) water column temperatures were recently shown to correlate well with brGDGTs in high-latitude sediment traps (*38*) and were used where available; point measurements of in situ water temperature were used otherwise. "low DO" was defined as DO < 1 mg/liter. For the three lakes in this study without a published DO profile, samples below a reported redox transition zone were considered as low DO (*53*, *77*).

Where available, in situ pH values were used for all sample types except riverine and lacustrine surface sediments, for which we used an average water column pH. For marine sediments, we used an average ocean pH of 8.1. However, we stress that this is only an approximation, especially because many sediments in the compiled dataset are from coastal margins at the outflows of major river systems, where pH can be both spatially and temporally variable [e.g., (*78*)].

Statistical analysis

All statistical analyses were performed in R (*79*). We generated quadratic (Fig. 3, D and G) or linear (all others) regressions for all relationships herein and in the figures. P values were <0.01 for all regressions in both the figures and the text or else are denoted by an asterisk (Figs. 3 and 4 and figs. S3 and S6) or an open point (figs. S2, S5, and S7). Primarily because of the low abundances of some compounds, some samples in Figs. 2, 3, 5A, and 6 displayed an FA = 0 or 1. These points, which are denoted by open circles in the plots, were not included in statistical analyses (r and n values, fitting coefficients, and plotted trend lines).

SUPPLEMENTARY MATERIALS

Supplementary material for this article is available at https://science.org/doi/10.1126/sciadv.abm7625

REFERENCES AND NOTES

1. S. Kusch, M. Winterfeld, G. Mollenhauer, S. T. Höfle, L. Schirrmeister, G. Schwamborn, J. Rethemeyer, Glycerol dialkyl glycerol tetraethers (GDGTs) in high latitude Siberian permafrost: Diversity, environmental controls, and implications for proxy applications. *Org. Geochem.* **136**, 103888 (2019).
2. W. Xiao, Y. Wang, Y. Liu, X. Zhang, L. Shi, Y. Xu, Predominance of hexamethylated 6-methyl branched glycerol dialkyl glycerol tetraethers in the Mariana Trench: Source and environmental implication. *Biogeosciences.* **17**, 2135–2148 (2020).

3. J. W. H. Weijers, S. Schouten, O. C. Spaargaren, J. S. Sinninghe Damsté, Occurrence and distribution of tetraether membrane lipids in soils: Implications for the use of the TEX86 proxy and the BIT index. *Org. Geochem.* **37**, 1680–1693 (2006).
4. J. S. S. Damsté, E. C. Hopmans, R. D. Pancost, S. Schouten, J. A. J. Geenevasen, Newly discovered non-isoprenoid glycerol dialkyl glycerol tetraether lipids in sediments. *Chem. Commun.* **0**, 1683–1684 (2000).
5. S. Ding, B. Kohlhepp, S. Trumbore, K. Küsel, K. U. Totsche, G. Pohnert, G. Gleixner, V. F. Schwab, In situ production of core and intact bacterial and archaeal tetraether lipids in groundwater. *Org. Geochem.* **126**, 1–12 (2018).
6. S. Schouten, M. T. J. Van Der Meer, E. C. Hopmans, W. I. C. Rijpstra, A. L. Reysenbach, D. M. Ward, J. S. S. Damsté, Archaeal and bacterial glycerol dialkyl glycerol tetraether lipids in hot springs of Yellowstone National Park. *Appl. Environ. Microbiol.* **73**, 6181–6191 (2007).
7. S. Fietz, F. G. Prahl, N. Moraleda, A. Rosell-Melé, Eolian transport of glycerol dialkyl glycerol tetraethers (GDGTs) off Northwest Africa. *Org. Geochem.* **64**, 112–118 (2013).
8. S. A. Lincoln, A. S. Bradley, S. A. Newman, R. E. Summons, Archaeal and bacterial glycerol dialkyl glycerol tetraether lipids in chimneys of the Lost City Hydrothermal Field. *Org. Geochem.* **60**, 45–53 (2013).
9. Z. X. Zhang, J. Li, Z. Chen, Z. Sun, H. Yang, M. Fu, X. Peng, The effect of methane seeps on the bacterial tetraether lipid distributions at the Okinawa Trough. *Mar. Chem.* **225**, 103845 (2020).
10. J. T. Dillon, S. Lash, J. Zhao, K. P. Smith, P. van Dommelen, A. K. Scherer, Y. Huang, Bacterial tetraether lipids in ancient bones record past climate conditions at the time of disposal. *J. Archaeol. Sci.* **96**, 45–56 (2018).
11. H. Yang, W. Ding, C. L. Zhang, X. Wu, X. Ma, G. He, J. Huang, S. Xie, Occurrence of tetraether lipids in stalagmites: Implications for sources and GDGT-based proxies. *Org. Geochem.* **42**, 108–115 (2011).
12. S. A. Newman, S. A. Lincoln, S. O'Reilly, X. Liu, E. L. Shock, P. B. Kelemen, R. E. Summons, Lipid biomarker record of the serpentinite-hosted ecosystem of the Samail Ophiolite, Oman and implications for the search for biosignatures on mars. *Astrobiology* **20**, 830–845 (2020).
13. J. E. Tierney, J. M. Russell, Distributions of branched GDGTs in a tropical lake system: Implications for lacustrine application of the MBT/CBT paleoproxy. *Org. Geochem.* **40**, 1032–1036 (2009).
14. C. De Jonge, A. Stadnitskaia, E. C. Hopmans, G. Cherkashov, A. Fedotov, J. S. Sinninghe Damsté, In situ produced branched glycerol dialkyl glycerol tetraethers in suspended particulate matter from the Yenisei River, Eastern Siberia. *Geochim. Cosmochim. Acta* **125**, 476–491 (2014).
15. E. C. Hopmans, J. W. H. Weijers, E. Schefuß, L. Herfort, J. S. S. Damsté, S. Schouten, A novel proxy for terrestrial organic matter in sediments based on branched and isoprenoid tetraether lipids. *Earth Planet. Sci. Lett.* **224**, 107–116 (2004).
16. C. I. Blaga, G.-J. J. Reichart, O. Heiri, J. S. S. Damsté, Tetraether membrane lipid distributions in water-column particulate matter and sediments: A study of 47 European lakes along a north-south transect. *J. Paleolimnol.* **41**, 523–540 (2009).
17. J. R. Super, K. Chin, M. Pagani, H. Li, C. Tabor, D. M. Harwood, P. M. Hull, Late cretaceous climate in the Canadian Arctic: Multi-proxy constraints from Devon Island. *Palaeogeogr. Palaeoclimatol. Palaeoecol.* **504**, 1–22 (2018).
18. B. D. A. Naafs, M. Rohrssen, G. N. Inglis, O. Lähteenoja, S. J. Feakins, M. E. Collinson, E. M. Kennedy, P. K. Singh, M. P. Singh, D. J. Lunt, R. D. Pancost, High temperatures in the terrestrial mid-latitudes during the Early Palaeogene. *Nat. Geosci.* **11**, 766–771 (2018).
19. H. Lu, W. Liu, H. Yang, H. Wang, Z. Liu, Q. Leng, Y. Sun, W. Zhou, Z. An, 800-kyr land temperature variations modulated by vegetation changes on Chinese Loess Plateau. *Nat. Commun.* **10**, 1–10 (2019).
20. S. E. Crump, G. H. Miller, M. Power, J. Sepúlveda, N. Dildar, M. Coghlan, M. Bunce, Arctic shrub colonization lagged peak postglacial warmth: Molecular evidence in lake sediment from Arctic Canada. *Glob. Chang. Biol.* **25**, 1–13 (2019).
21. D. J. Harning, L. Curtin, Á. Geirsdóttir, W. J. D'Andrea, G. H. Miller, J. Sepúlveda, Lipid biomarkers quantify holocene summer temperature and ice cap sensitivity in icelandic lakes. *Geophys. Res. Lett.* **47**, 1–11 (2020).
22. J. W. H. Weijers, E. Schefuß, S. Schouten, J. S. Sinninghe Damsté, Coupled thermal and hydrological evolution of tropical Africa over the last deglaciation. *Science (80-.).* **315**, 1701–1704 (2007).
23. E. Dearing Crampton-Flood, F. Peterse, D. Munsterman, J. S. Sinninghe Damsté, Using tetraether lipids archived in North Sea Basin sediments to extract North Western European Pliocene continental air temperatures. *Earth Planet. Sci. Lett.* **490**, 193–205 (2018).
24. J. W. H. Weijers, S. Schouten, J. C. Van Den Donker, E. C. Hopmans, J. C. van den Donker, E. C. Hopmans, J. S. Sinninghe Damsté, Environmental controls on bacterial tetraether membrane lipid distribution in soils. *Geochim. Cosmochim. Acta* **71**, 703–713 (2007).
25. C. De Jonge, D. Radujković, B. D. Sigurdsson, J. T. Weedon, I. Janssens, F. Peterse, Lipid biomarker temperature proxy responds to abrupt shift in the bacterial community composition in geothermally heated soils. *Org. Geochem.* **137**, 103897 (2019).
26. Y. Weber, J. S. S. Damsté, J. Zopfi, C. De Jonge, A. Gilli, C. J. Schubert, F. Lepori, M. F. Lehmann, H. Niemann, Redox-dependent niche differentiation provides evidence for multiple bacterial sources of glycerol tetraether lipids in lakes. *Proc. Natl. Acad. Sci. U.S.A.* **115**, 10926–10931 (2018).
27. L. G. J. Van Bree, F. Peterse, A. J. Baxter, W. De Crop, S. Van Grinsven, L. Villanueva, D. Verschuren, J. S. Sinninghe Damsté, Seasonal variability and sources of in situ brGDGT production in a permanently stratified African crater lake. *Biogeosciences.* **17**, 5443–5463 (2020).
28. C. De Jonge, E. E. Kuramae, D. Radujković, J. T. Weedon, I. A. Janssens, F. Peterse, The influence of soil chemistry on branched tetraether lipids in mid- and high latitude soils: Implications for brGDGT- based paleothermometry. *Geochim. Cosmochim. Acta* **310**, 95–112 (2021).
29. J. Wu, H. Yang, R. D. Pancost, B. D. A. Naafs, S. Qian, X. Dang, H. Sun, H. Pei, R. Wang, S. Zhao, S. Xie, Variations in dissolved O2 in a Chinese lake drive changes in microbial communities and impact sedimentary GDGT distributions. *Chem. Geol.* **579**, 120348 (2021).
30. J. S. Sinninghe Damsté, W. I. C. Rijpstra, B. U. Foesel, K. J. Huber, J. Overmann, S. Nakagawa, J. J. Kim, P. F. Dunfield, S. N. Dedysh, L. Villanueva, An overview of the occurrence of ether- and ester-linked iso-diabolic acid membrane lipids in microbial cultures of the Acidobacteria: Implications for brGDGT paleoproxies for temperature and pH. *Org. Geochem.* **124**, 63–76 (2018).
31. J. S. Sinninghe Damsté, W. I. C. Rijpstra, E. C. Hopmans, J. W. H. Weijers, B. U. Foesel, J. Overmann, S. N. Dedysh, 13,16-Dimethyl octacosanedioic acid (iso-diabolic acid), a common membrane-spanning lipid of acidobacteria subdivisions 1 and 3. *Appl. Environ. Microbiol.* **77**, 4147–4154 (2011).
32. T. A. Halamka, J. M. McFarlin, A. D. Younkin, J. Depoy, N. Dildar, S. H. Kopf, Oxygen limitation can trigger the production of branched GDGTs in culture. *Geochemical Perspect. Lett.* , 36–39 (2021).
33. Y. Chen, F. Zheng, S. Chen, H. Liu, T. J. Phelps, C. Zhang, Branched GDGT production at elevated temperatures in anaerobic soil microcosm incubations. *Org. Geochem.* **117**, 12–21 (2018).
34. P. Martínez-Sosa, J. E. Tierney, L. K. Meredith, Controlled lacustrine microcosms show a brGDGT response to environmental perturbations. *Org. Geochem.* **145**, 104041 (2020).
35. B. D. A. Naafs, A. S. F. Oliveira, A. J. Mulholland, Molecular dynamics simulations support the hypothesis that the brGDGT paleothermometer is based on homeoviscous adaptation. *Geochim. Cosmochim. Acta* **312**, 44–56 (2021).
36. E. Dearing Crampton-Flood, J. E. Tierney, F. Peterse, F. M. S. A. Kirkels, J. S. Sinninghe Damsté, BayMBT: A Bayesian calibration model for branched glycerol dialkyl glycerol tetraethers in soils and peats. *Geochim. Cosmochim. Acta* **268**, 142–159 (2020).
37. P. Martínez-Sosa, J. E. Tierney, I. C. Stefanescu, E. Dearing Crampton-Flood, B. N. Shuman, C. Routson, A global Bayesian temperature calibration for lacustrine brGDGTs. *Geochim. Cosmochim. Acta* **305**, 87–105 (2021).
38. B. Zhao, I. S. Castañeda, R. S. Bradley, J. M. Salacup, G. A. de Wet, W. C. Daniels, T. Schneider, Development of an in situ branched GDGT calibration in Lake 578, southern Greenland. *Org. Geochem.* **152**, 104168 (2021).
39. J. Zhao, Y. Huang, Y. Yao, Z. An, Y. Zhu, H. Lu, Z. Wang, Calibrating branched GDGTs in bones to temperature and precipitation: Application to Alaska chronological sequences. *Quat. Sci. Rev.* **240**, 106371 (2020).
40. A. J. Blyth, S. Schouten, Calibrating the glycerol dialkyl glycerol tetraether temperature signal in speleothems. *Geochim. Cosmochim. Acta* **109**, 312–328 (2013).
41. J. M. Russell, E. C. Hopmans, S. E. Loomis, J. Liang, J. S. Sinninghe Damsté, Distributions of 5- and 6-methyl branched glycerol dialkyl glycerol tetraethers (brGDGTs) in East African lake sediment: Effects of temperature, pH, and new lacustrine paleotemperature calibrations. *Org. Geochem.* **117**, 56–69 (2018).
42. X. Dang, W. Ding, H. Yang, R. D. Pancost, B. D. A. Naafs, J. Xue, X. Lin, J. Lu, S. Xie, Different temperature dependence of the bacterial brGDGT isomers in 35 Chinese lake sediments compared to that in soils. *Org. Geochem.* **119**, 72–79 (2018).
43. E. Dearing Crampton-Flood, C. M. H. van der Weijst, G. van der Molen, M. Bouquet, Y. Yedema, T. H. Donders, F. Sangiorgi, A. Sluijs, J. S. Sinninghe Damsté, F. Peterse, Identifying marine and freshwater overprints on soil-derived branched GDGT temperature signals in Pliocene Mississippi and Amazon River fan sediments. *Org. Geochem.* **154**, 104200 (2021).
44. C. De Jonge, A. Stadnitskaia, E. C. Hopmans, G. Cherkashov, A. Fedotov, I. D. Streletskaya, A. A. Vasiliev, J. S. Sinninghe Damsté, Drastic changes in the distribution of branched tetraether lipids in suspended matter and sediments from the Yenisei River and Kara Sea (Siberia): Implications for the use of brGDGT-based proxies in coastal marine sediments. *Geochim. Cosmochim. Acta* **165**, 200–225 (2015).
45. L. K. Buckles, J. W. H. Weijers, X.-M. Tran, S. Waldron, J. S. Sinninghe Damsté, Provenance of tetraether membrane lipids in a large temperate lake (Loch Lomond, UK): Implications for glycerol dialkyl glycerol tetraether (GDGT)-based palaeothermometry. *Biogeosciences.* **11**, 5539–5563 (2014).

46. S. E. Loomis, J. M. Russell, A. M. Heureux, W. J. D'Andrea, J. S. Sinninghe Damsté, Seasonal variability of branched glycerol dialkyl glycerol tetraethers (brGDGTs) in a temperate lake system. *Geochim. Cosmochim. Acta* **144**, 173–187 (2014).
47. J. Guo, M. Glendell, J. Meersmans, F. Kirkels, J. J. Middelburg, F. Peterse, Assessing branched tetraether lipids as tracers of soil organic carbon transport through the Carminowe Creek catchment (southwest England). *Biogeosciences.* **17**, 3183–3201 (2020).
48. J. S. Sinninghe Damsté, Spatial heterogeneity of sources of branched tetraethers in shelf systems: The geochemistry of tetraethers in the Berau River delta (Kalimantan, Indonesia). *Geochim. Cosmochim. Acta* **186**, 13–31 (2016).
49. S. Xie, X. L. Liu, F. Schubotz, S. G. Wakeham, K. U. Hinrichs, Distribution of glycerol ether lipids in the oxygen minimum zone of the Eastern Tropical North Pacific Ocean. *Org. Geochem.* **71**, 60–71 (2014).
50. L. Dugerdil, S. Joannin, O. Peyron, I. Jouffroy-Bapicot, B. Vannière, B. Boldgiv, J. Unkelbach, H. Behling, G. Ménot, Climate reconstructions based on GDGT and pollen surface datasets from Mongolia and Baikal area: Calibrations and applicability to extremely cold-dry environments over the Late Holocene. *Clim. Past.* **17**, 1199–1226 (2021).
51. J. Lattaud, C. De Jonge, A. Pearson, F. J. Elling, T. I. Eglinton, Microbial lipid signatures in Arctic deltaic sediments–Insights into methane cycling and climate variability. *Org. Geochem.* **157**, 104242 (2021).
52. D. E. Colcord, A. Pearson, S. C. Brassell, Carbon isotopic composition of intact branched GDGT core lipids in Greenland lake sediments and soils. *Org. Geochem.* **110**, 25–32 (2017).
53. Y. Yao, J. Zhao, R. S. Vachula, J. P. Werne, J. Wu, X. Song, Y. Huang, Correlation between the ratio of 5-methyl hexamethylated to pentamethylated branched GDGTs (HP5) and water depth reflects redox variations in stratified lakes. *Org. Geochem.* **147**, 104076 (2020).
54. X. L. Liu, C. Zhu, S. G. Wakeham, K. U. Hinrichs, In situ production of branched glycerol dialkyl glycerol tetraethers in anoxic marine water columns. *Mar. Chem.* **166**, 1–8 (2014).
55. J. H. Raberg, D. J. Harning, S. E. Crump, G. De Wet, A. Blumm, S. Kopf, Á. Geirsdóttir, G. H. Miller, J. Sepúlveda, Revised fractional abundances and warm-season temperatures substantially improve brGDGT calibrations in lake sediments. *Biogeosciences.* **18**, 3579–3603 (2021).
56. H. Wang, W. Liu, Y. He, A. Zhou, H. Zhao, H. Liu, Y. Cao, J. Hu, B. Meng, J. Jiang, M. Kolpakova, S. Krivonogov, Z. Liu, Salinity-controlled isomerization of lacustrine brGDGTs impacts the associated MBT5ME′ terrestrial temperature index. *Geochim. Cosmochim. Acta* **305**, 33–48 (2021).
57. J.-H. Kim, C. Zell, P. Moreira-Turcq, M. A. P. Pérez, G. Abril, J.-M. Mortillaro, J. W. H. Weijers, T. Meziane, J. S. Sinninghe Damsté, Tracing soil organic carbon in the lower amazon river and its tributaries using GDGT distributions and bulk organic matter properties. *Geochim. Cosmochim. Acta* **90**, 163–180 (2012).
58. J. Hu, H. Zhou, P. Peng, B. Spiro, Seasonal variability in concentrations and fluxes of glycerol dialkyl glycerol tetraethers in Huguangyan Maar Lake, SE China: Implications for the applicability of the MBT-CBT paleotemperature proxy in lacustrine settings. *Chem. Geol.* **420**, 200–212 (2016).
59. S. E. Loomis, J. M. Russell, H. Eggermont, D. Verschuren, J. S. Sinninghe Damsté, Effects of temperature, pH and nutrient concentration on branched GDGT distributions in East African lakes: Implications for paleoenvironmental reconstruction. *Org. Geochem.* **66**, 25–37 (2014).
60. T. M. Shanahan, K. A. Hughen, B. A. S. Van Mooy, Temperature sensitivity of branched and isoprenoid GDGTs in Arctic lakes. *Org. Geochem.* **64**, 119–128 (2013).
61. B. D. A. Naafs, A. V. Gallego-Sala, G. N. Inglis, R. D. Pancost, Refining the global branched glycerol dialkyl glycerol tetraether (brGDGT) soil temperature calibration. *Org. Geochem.* **106**, 48–56 (2017).
62. L. C. P.-Angel, J. Sepúlveda, P. Molnar, C. Montes, B. Rajagopalan, K. Snell, C. G.-Arango, N. Dildar, Soil and air temperature calibrations using branched GDGTs for the tropical andes of colombia: Toward a pan-tropical calibration. *Geochemistry, Geophys. Geosystems.* **21**, 1–18 (2020).
63. H. Wang, Z. An, H. Lu, Z. Zhao, W. Liu, Calibrating bacterial tetraether distributions towards in situ soil temperature and application to a loess-paleosol sequence. *Quat. Sci. Rev.* **231**, 106172 (2020).
64. H. Pei, C. Wang, Y. Wang, H. Yang, S. Xie, Distribution of microbial lipids at an acid mine drainage site in China: Insights into microbial adaptation to extremely low pH conditions. *Org. Geochem.* **134**, 77–91 (2019).
65. C. De Jonge, E. C. Hopmans, C. I. Zell, J. H. Kim, S. Schouten, J. S. Sinninghe Damsté, Occurrence and abundance of 6-methyl branched glycerol dialkyl glycerol tetraethers in soils: Implications for palaeoclimate reconstruction. *Geochim. Cosmochim. Acta* **141**, 97–112 (2014).
66. X. Y. Dang, J. T. Xue, H. Yang, S. C. Xie, Environmental impacts on the distribution of microbial tetraether lipids in Chinese lakes with contrasting pH: Implications for lacustrine paleoenvironmental reconstructions. *Sci. China Earth Sci.* **59**, 939–950 (2016).
67. C. Gao, Y. Yang, H. Yang, Y. G. Zhang, X. Lü, H. Wang, X. Yu, X. Ruan, Different temperature dependence of marine-derived brGDGT isomers in a sediment core from the Chukchi Sea shelf. *Org. Geochem.* **152**, 104169 (2021).
68. Y. Liu, W. Xiao, J. Wu, L. Han, H. Zhang, Y. Xu, Source, composition, and distributional pattern of branched tetraethers in sediments of northern Chinese marginal seas. *Org. Geochem.* **157**, 104244 (2021).
69. I. C. Stefanescu, B. N. Shuman, J. E. Tierney, Temperature and water depth effects on brGDGT distributions in sub-alpine lakes of mid-latitude North America. *Org. Geochem.* **152**, 104174 (2021).
70. P. C. Baveye, W. Otten, A. Kravchenko, M. B.-Romero, É. Beckers, M. Chalhoub, C. Darnault, T. Eickhorst, P. Garnier, S. Hapca, S. Kiranyaz, O. Monga, C. W. Mueller, N. Nunan, V. Pot, S. Schlüter, H. Schmidt, H.-J. Vogel, Emergent properties of microbial activity in heterogeneous soil microenvironments: Different research approaches are slowly converging, yet major challenges remain. *Front. Microbiol.* **9**, 1929 (2018).
71. E. D. C.-Flood, F. Peterse, J. S. S. Damsté, Production of branched tetraethers in the marine realm: Svalbard fjord sediments revisited. *Org. Geochem.* **138**, 103907 (2019).
72. J. J. Lembrechts, J. van den Hoogen, J. Aalto, M. B. Ashcroft, P. De Frenne, J. Kemppinen, M. Kopecký, M. Luoto, I. M. D. Maclean, T. W. Crowther, J. J. Bailey, S. Haesen, D. H. Klinges, P. Niittynen, B. R. Scheffers, K. Van Meerbeek, P. Aartsma, O. Abdalaze, M. Abedi, R. Aerts, N. Ahmadian, A. Ahrends, J. M. Alatalo, J. M. Alexander, C. N. Allonsius, J. Altman, C. Ammann, C. Andres, C. Andrews, J. Ardö, N. Arriga, A. Arzac, V. Aschero, R. L. Assis, J. J. Assmann, M. Y. Bader, K. Bahalkeh, P. Barančok, I. C. Barrio, A. Barros, M. Barthel, E. W. Basham, M. Bauters, M. Bazzichetto, L. B. Marchesini, M. C. Bell, J. C. Benavides, J. L. B. Alonso, B. J. Berauer, J. W. Bjerke, R. G. Björk, M. P. Björkman, K. Björnsdóttir, B. Blonder, P. Boeckx, J. Boike, S. Bokhorst, B. N. S. Brum, J. Brůna, N. Buchmann, P. Buysse, J. L. Camargo, O. C. Campoe, O. Candan, R. Canessa, N. Cannone, M. Carbognani, J. Carnicer, A. C.-Katny, S. Cesarz, B. Chojnicki, P. Choler, S. L. Chown, E. F. Cifuentes, M. Čiliak, T. Contador, P. Convey, E. J. Cooper, E. Cremonese, S. R. Curasi, R. Curtis, M. Cutini, C. J. Dahlberg, G. N. Daskalova, M. A. de Pablo, S. D. Chiesa, J. Dengler, B. Deronde, P. Descombes, V. Di Cecco, M. Di Musciano, J. Dick, R. D. Dimarco, J. Dolezal, E. Dorrepaal, J. Dušek, N. Eisenhauer, L. Eklundh, T. E. Erickson, B. Erschbamer, W. Eugster, R. M. Ewers, D. A. Exton, N. Fanin, F. Fazlioglu, I. Feigenwinter, G. Fenu, O. Ferlian, M. R. F. Calzado, E. F.-Pascual, M. Finckh, R. F. Higgens, T. G. W. Forte, E. C. Freeman, E. R. Frei, E. F.-Lillo, R. A. García, M. B. García, C. Géron, M. Gharun, D. Ghosn, K. Gigauri, A. Gobin, I. Goded, M. Goeckede, F. Gottschall, K. Goulding, S. Govaert, B. J. Graae, S. Greenwood, C. Greiser, A. Grelle, B. Guénard, M. Guglielmin, J. Guillemot, P. Haase, S. Haider, A. H. Halbritter, M. Hamid, A. Hammerle, A. Hampe, S. V. Haugum, L. Hederová, B. Heinesch, C. Helfter, D. Hepenstrick, M. Herberich, M. Herbst, L. Hermanutz, D. S. Hik, R. Hoffrén, J. Homeier, L. Hörtnagl, T. T. Høye, F. Hrbacek, K. Hylander, H. Iwata, M. A. J.-korczynski, H. Jactel, J. Järveoja, S. Jastrzębowski, A. Jentsch, J. J. Jiménez, I. S. Jónsdóttir, T. Jucker, A. S. Jump, R. Juszczak, R. Kanka, V. Kašpar, G. Kazakis, J. Kelly, A. A. Khuroo, L. Klemedtsson, M. Klisz, N. Kljun, A. Knohl, J. Kobler, J. Kollár, M. M. Kotowska, B. Kovács, J. Kreyling, A. Lamprecht, S. I. Lang, C. Larson, K. Larson, K. Laska, G. le Maire, R. I. Leihy, L. Lens, B. Liljebladh, A. Lohila, J. Lorite, B. Loubet, J. Lynn, M. Macek, R. Mackenzie, E. Magliulo, R. Maier, F. Malfasi, F. Máliš, M. Man, G. Manca, A. Manco, T. Manise, P. Manolaki, F. Marciniak, R. Matula, A. C. Mazzolari, S. Medinets, V. Medinets, C. Meeussen, S. Merinero, R. de C. G. Mesquita, K. Meusburger, F. J. R. Meysman, S. T. Michaletz, A. Milbau, D. Moiseev, P. Moiseev, A. Mondoni, R. Monfries, L. Montagnani, M. M.-Armendariz, U. M. di Cella, M. Mörsdorf, J. R. Mosedale, L. Muffler, M. M.-Rojas, J. A. Myers, I. H. M.-Smith, L. Nagy, M. Nardino, I. Naujokaitis-Lewis, E. Newling, L. Nicklas, G. Niedrist, A. Niessner, M. B. Nilsson, S. Normand, M. D. Nosetto, Y. Nouvellon, M. A. Nuñez, R. Ogaya, J. Ogée, J. Okello, J. Olejnik, J. E. Olesen, Ø. Opedal, S. Orsenigo, A. Palaj, T. Pampuch, A. V. Panov, M. Pärtel, A. Pastor, A. Pauchard, H. Pauli, M. Pavelka, W. D. Pearse, M. Peichl, L. Pellissier, R. M. Penczykowski, J. Penuelas, M. P. Bon, A. Petraglia, S. S. Phartyal, G. K. Phoenix, C. Pio, A. Pitacco, C. Pitteloud, R. Plichta, F. Porro, M. P.-Estrada, J. Poulenard, R. Poyatos, A. S. Prokushkin, R. Puchalka, M. Puşcaş, D. Radujković, K. Randall, A. R. Backes, S. Remmele, W. Remmers, D. Renault, A. C. Risch, C. Rixen, S. A. Robinson, B. J. M. Robroek, A. V. Rocha, C. Rossi, G. Rossi, O. Roupsard, A. V. Rubtsov, P. Saccone, C. Sagot, J. S. Bravo, C. C. Santos, J. M. Sarneel, T. Scharnweber, J. Schmeddes, M. Schmidt, T. Scholten, M. Schuchardt, N. Schwartz, T. Scott, J. Seeber, A. C. S. de Andrade, T. Seipel, P. Semenchuk, R. A. Senior, J. M. Serra-Diaz, P. Sewerniak, A. Shekhar, N. V. Sidenko, L. Siebicke, L. S. Collier, E. Simpson, D. P. Siqueira, Z. Sitková, J. Six, M. Smiljanic, S. W. Smith, S. Smith-Tripp, B. Somers, M. V. Sørensen, J. J. L. L. Souza, B. I. Souza, A. S. Dias, M. J. Spasojevic, J. D. M. Speed, F. Spicher, A. Stanisci, K. Steinbauer, R. Steinbrecher, M. Steinwandter, M. Stemkovski, J. G. Stephan, C. Stiegler, S. Stoll, M. Svátek, M. Svoboda, T. Tagesson, A. J. Tanentzap, F. Tanneberger, J.-P. J. J.-P. Theurillat, H. J. D. Thomas, A. D. Thomas, K. Tielbörger, M. Tomaselli, U. A. Treier, M. Trouillier, P. D. Turtureanu, R. Tutton, V. A. Tyystjärvi, M. Ueyama, K. Ujházy, M. Ujházyová, D. Uogintas, A. V. Urban, J. Urban, M. Urbaniak, T.-M. T. Ursu, F. P. Vaccari, S. Van de Vondel, L. van den Brink, M. Van Geel, V. Vandvik, P. Vangansbeke, A. Varlagin, G. F. Veen, E. Veenendaal, S. E. Venn, H. Verbeeck, E. Verbrugggen, F. G. A. Verheijen,

L. Villar, L. Vitale, P. Vittoz, M. V.-Ingla, J. von Oppen, J. Walz, R. Wang, Y. Wang, R. G. Way, R. E. M. Wedegärtner, R. Weigel, J. Wild, M. Wilkinson, M. Wilmking, L. Wingate, M. Winkler, S. Wipf, G. Wohlfahrt, G. Xenakis, Y. Yang, Z. Yu, K. Yu, F. Zellweger, J. Zhang, Z. Zhang, P. Zhao, K. Ziemblińska, R. Zimmermann, S. Zong, V. I. Zyryanov, I. Nijs, J. Lenoir, J. van den Hoogen, J. Aalto, M. B. Ashcroft, P. De Frenne, J. Kemppinen, M. Kopecký, M. Luoto, I. M. D. Maclean, T. W. Crowther, J. J. Bailey, S. Haesen, D. H. Klinges, P. Niittynen, B. R. Scheffers, K. Van Meerbeek, P. Aartsma, O. Abdalaze, M. Abedi, R. Aerts, N. Ahmadian, A. Ahrends, J. M. Alatalo, J. M. Alexander, C. N. Allonsius, J. Altman, C. Ammann, C. Andres, C. Andrews, J. Ardö, N. Arriga, A. Arzac, V. Aschero, R. L. Assis, J. J. Assmann, M. Y. Bader, K. Bahalkeh, P. Barančok, I. C. Barrio, A. Barros, M. Barthel, E. W. Basham, M. Bauters, M. Bazzichetto, L. B. Marchesini, M. C. Bell, J. C. Benavides, J. L. B. Alonso, B. J. Berauer, J. W. Bjerke, R. G. Björk, M. P. Björkman, K. Björnsdóttir, B. Blonder, P. Boeckx, J. Boike, S. Bokhorst, B. N. S. Brum, J. Brůna, N. Buchmann, P. Buysse, J. L. Camargo, O. C. Campoe, O. Candan, R. Canessa, N. Cannone, M. Carbognani, J. Carnicer, A. C.-Katny, S. Cesarz, B. Chojnicki, P. Choler, S. L. Chown, E. F. Cifuentes, M. Čiliak, T. Contador, P. Convey, E. J. Cooper, E. Cremonese, S. R. Curasi, R. Curtis, M. Cutini, C. J. Dahlberg, G. N. Daskalova, M. A. de Pablo, S. D. Chiesa, J. Dengler, B. Deronde, P. Descombes, V. Di Cecco, M. Di Musciano, J. Dick, R. D. Dimarco, J. Dolezal, E. Dorrepaal, J. Dušek, N. Eisenhauer, L. Eklundh, T. E. Erickson, B. Erschbamer, W. Eugster, R. M. Ewers, D. A. Exton, N. Fanin, F. Fazlioglu, I. Feigenwinter, G. Fenu, O. Ferlian, M. R. F. Calzado, E. F.-Pascual, M. Finckh, R. F. Higgens, T. G. W. Forte, E. C. Freeman, E. R. Frei, E. F.-Lillo, R. A. García, M. B. García, C. Géron, M. Gharun, D. Ghosn, K. Gigauri, A. Gobin, I. Goded, M. Goeckede, F. Gottschall, K. Goulding, S. Govaert, B. J. Graae, S. Greenwood, C. Greiser, A. Grelle, B. Guénard, M. Guglielmin, J. Guillemot, P. Haase, S. Haider, A. H. Halbritter, M. Hamid, A. Hammerle, A. Hampe, S. V. Haugum, L. Hederová, B. Heinesch, C. Helfter, D. Hepenstrick, M. Herberich, M. Herbst, L. Hermanutz, D. S. Hik, R. Hoffrén, J. Homeier, L. Hörtnagl, T. T. Høye, F. Hrbacek, K. Hylander, H. Iwata, M. A. J.-Korczynski, H. Jactel, J. Järveoja, S. Jastrzębowski, A. Jentsch, J. J. Jiménez, I. S. Jónsdóttir, T. Jucker, A. S. Jump, R. Juszczak, R. Kanka, V. Kašpar, G. Kazakis, J. Kelly, A. A. Khuroo, L. Klemedtsson, M. Klisz, N. Kljun, A. Knohl, J. Kobler, J. Kollár, M. M. Kotowska, B. Kovács, J. Kreyling, A. Lamprecht, S. I. Lang, C. Larson, K. Larson, K. Laska, G. le Maire, R. I. Leihy, L. Lens, B. Liljebladh, A. Lohila, J. Lorite, B. Loubet, J. Lynn, M. Macek, R. Mackenzie, E. Magliulo, R. Maier, F. Malfasi, F. Máliš, M. Man, G. Manca, A. Manco, T. Manise, P. Manolaki, F. Marciniak, R. Matula, A. C. Mazzolari, S. Medinets, V. Medinets, C. Meeussen, S. Merinero, R. de C. G. Mesquita, K. Meusburger, F. J. R. Meysman, S. T. Michaletz, A. Milbau, D. Moiseev, P. Moiseev, A. Mondoni, R. Monfries, L. Montagnani, M. M.-Armendariz, U. M. di Cella, M. Mörsdorf, J. R. Mosedale, L. Muffler, M. M.-Rojas, J. A. Myers, I. H. Myers-Smith, L. Nagy, M. Nardino, I. N.-Lewis, E. Newling, L. Nicklas, G. Niedrist, A. Niessner, M. B. Nilsson, S. Normand, M. D. Nosetto, Y. Nouvellon, M. A. Nuñez, R. Ogaya, J. Ogée, J. Okello, J. Olejnik, J. E. Olesen, Ø. Opedal, S. Orsenigo, A. Palaj, T. Pampuch, A. V. Panov, M. Pärtel, A. Pastor, A. Pauchard, H. Pauli, M. Pavelka, W. D. Pearse, M. Peichl, L. Pellissier, R. M. Penczykowski, J. Penuelas, M. P. Bon, A. Petraglia, S. S. Phartyal, G. K. Phoenix, C. Pio, A. Pitacco, C. Pitteloud, R. Plichta, F. Porro, M. P.-Estrada, J. Poulenard, R. Poyatos, A. S. Prokushkin, R. Puchalka, M. Puşcaş, D. Radujković, K. Randall, A. R. Backes, S. Remmele, W. Remmers, D. Renault, A. C. Risch, C. Rixen, S. A. Robinson, B. J. M. Robroek, A. V. Rocha, C. Rossi, G. Rossi, O. Roupsard, A. V. Rubtsov, P. Saccone, C. Sagot, J. S. Bravo, C. C. Santos, J. M. Sarneel, T. Scharnweber, J. Schmeddes, M. Schmidt, T. Scholten, M. Schuchardt, N. Schwartz, T. Scott, J. Seeber, A. C. S. de Andrade, T. Seipel, P. Semenchuk, R. A. Senior, J. M. S.-Diaz, P. Sewerniak, A. Shekhar, N. V. Sidenko, L. Siebicke, L. S. Collier, E. Simpson, D. P. Siqueira, Z. Sitková, J. Six, M. Smiljanic, S. W. Smith, S. S.-Tripp, B. Somers, M. V. Sørensen, J. J. L. L. Souza, B. I. Souza, A. S. Dias, M. J. Spasojevic, J. D. M. Speed, F. Spicher, A. Stanisci, K. Steinbauer, R. Steinbrecher, M. Steinwandter, M. Stemkovski, J. G. Stephan, C. Stiegler, S. Stoll, M. Svátek, M. Svoboda, T. Tagesson, A. J. Tanentzap, F. Tanneberger, J.-P. J. J.-P. Theurillat, H. J. D. Thomas, A. D. Thomas, K. Tielbörger, M. Tomaselli, U. A. Treier, M. Trouillier, P. D. Turtureanu, R. Tutton, V. A. Tyystjärvi, M. Ueyama, K. Ujházy, M. Ujházyová, D. Uogintas, A. V. Urban, J. Urban, M. Urbaniak, T.-M. T. Ursu, F. P. Vaccari, S. Van de Vondel, L. van den Brink, M. Van Geel, V. Vandvik, P. Vangansbeke, A. Varlagin, G. F. Veen, E. Veenendaal, S. E. Venn, H. Verbeeck, E. Verbrugggen, F. G. A. Verheijen, L. Villar, L. Vitale, P. Vittoz, M. V.-Ingla, J. von Oppen, J. Walz, R. Wang, Y. Wang, R. G. Way, R. E. M. Wedegärtner, R. Weigel, J. Wild, M. Wilkinson, M. Wilmking, L. Wingate, M. Winkler, S. Wipf, G. Wohlfahrt, G. Xenakis, Y. Yang, Z. Yu, K. Yu, F. Zellweger, J. Zhang, Z. Zhang, P. Zhao, K. Ziemblińska, R. Zimmermann, S. Zong, V. I. Zyryanov, I. Nijs, J. Lenoir, M. Kopeck, M. Luoto, I. M. D. Maclean, T. W. Crowther, J. J. Bailey, S. O. Abdalaze, M. Abedi, R. Aerts, N. Ahmadian, A. Ahrends, J. M. Alatalo, J. M. Alexander, C. N. Allonsius, J. Altman, C. Ammann, C. Andres, C. Andrews, J. Ard, N. Arriga, A. Arzac, V. Aschero, R. L. Assis, J. J. Assmann, E. W. Basham, M. Bauters, M. Bazzichetto, L. B. Marchesini, M. C. Bell, J. C. Benavides, L. B. Alonso, B. J. Berauer, J. W. Bjerke, R. G. Bj, M. P. Bj, K. Bj, B. Blonder, P. Boeckx, J. Boike, S. Bokhorst, R. Canessa, N. Cannone, M. Carbognani, J. Carnicer, C. -Katny, S. Cesarz, B. Chojnicki, P. Choler, S. L. Chown, E. F. Cifuentes, T. Contador, P. Convey, E. J. Cooper, E. Cremonese, S. R. Curasi, R. Curtis, M. Cutini, J. Dahlberg, G. N. Daskalova, M. Angel, S. D. Chiesa, B. Deronde, P. Descombes, V. Di Cecco, M. Di Musciano, J. Dick, R. D. Dimarco, J. Dolezal, E. Dorrepaal, N. Eisenhauer, L. Eklundh, T. E. Erickson, B. Erschbamer, W. Eugster, R. M. Ewers, D. A. Exton, N. Fanin, D. H. Klinges, P. Niittynen, B. R. Scheffers, K. Van Meerbeek, P. Aartsma, M. Y. Bader, K. Bahalkeh, P. Baran, I. C. Barrio, A. Barros, M. Barthel, J. Br, N. Buchmann, P. Buysse, O. F. Fazlioglu, I. Feigenwinter, G. Fenu, O. Ferlian, R. Fern, E. Fern, M. Finckh, R. F. Higgens, E. C. Freeman, E. R. Frei, E. F.-Lillo, R. A. Garc, M. Gharun, D. Ghosn, K. Gigauri, A. Gobin, I. Goded, M. Goeckede, F. Gottschall, K. Goulding, S. Govaert, B. J. Graae, S. Greenwood, C. Greiser, A. Grelle, B. Gu, M. Guglielmin, P. Haase, S. Haider, A. H. Halbritter, M. Hamid, A. Hammerle, A. Hampe, S. V. Haugum, L. Hederov, B. Heinesch, C. Helfter, D. Hepenstrick, M. Herberich, M. Herbst, L. Hermanutz, D. S. Hik, F. Hrbacek, K. Hylander, H. Iwata, M. A. Jackowicz-korczynski, S. Jastrz, A. Jentsch, J. J. Jim, T. Jucker, A. S. Jump, R. Juszczak, G. Kazakis, J. Kelly, A. A. Khuroo, L. Klemedtsson, M. Klisz, N. Kljun, A. Knohl, J. Kobler, Global maps of soil temperature. *Glob. Chang. Biol.* **28**, 3110–3144 (2021).

73. J. H. Raberg, G. H. Miller, Á. Geirsdóttir, J. Sepúlveda, Global compilation of brGDGT lipid distributions, temperature, and pH across a dozen sample types. *PANGAEA* 10.1594/PANGAEA.940052 (2022).
74. S. E. Fick, R. J. Hijmans, WorldClim 2: New 1-km spatial resolution climate surfaces for global land areas. *Int. J. Climatol.* **37**, 4302–4315 (2017).
75. C. Zhu, J. W. H. Weijers, T. Wagner, J. M. Pan, J. F. Chen, R. D. Pancost, Sources and distributions of tetraether lipids in surface sediments across a large river-dominated continental margin. *Org. Geochem.* **42**, 376–386 (2011).
76. B. Huang, P. W. Thorne, V. F. Banzon, T. Boyer, G. Chepurin, J. H. Lawrimore, M. J. Menne, T. M. Smith, R. S. Vose, H.-M. Zhange, NOAA Extended reconstructed sea surface temperature (ERSST), version 5. (NOAA National Centers for Environmental Information, 2017).
77. Y. Yao, J. Zhao, T. Bauersachs, Y. Huang, Effect of water depth on the TEX 86 proxy in volcanic lakes of northeastern China. *Org. Geochem.* **129**, 88–98 (2019).
78. C. T. A. Chen, W. Zhai, M. Dai, Riverine input and air-sea CO2 exchanges near the Changjiang (Yangtze River) Estuary: Status quo and implication on possible future changes in metabolic status. *Cont. Shelf Res.* **28**, 1476–1482 (2008).
79. Team R Development Core, R: A language and environment for statistical computing. 2 (*R Found. Stat. Comput. 2*, 2021). www.r-project.org.
80. J. Cao, Z. Rao, F. Shi, G. Jia, Ice formation on lake surfaces in winter causes warm-season bias of lacustrine brGDGT temperature estimates. *Biogeosciences.* **17**, 2521–2536 (2020).
81. P. Martínez-Sosa, J. E. Tierney, Lacustrine brGDGT response to microcosm and mesocosm incubations. *Org. Geochem.* **127**, 12–22 (2019).
82. D. R. Miller, M. H. Habicht, B. A. Keisling, I. S. Castañeda, R. S. Bradley, A 900-year new england temperature reconstruction from in situ seasonally produced branched glycerol dialkyl glycerol tetraethers (brGDGTs). *Clim. Past.* **14**, 1653–1667 (2018).
83. L. Dugerdil, G. Ménot, O. Peyron, I. Jouffroy-Bapicot, S. Ansanay-Alex, I. Antheaume, H. Behling, B. Boldgiv, A. L. Develle, V. Grossi, J. Magail, M. Makou, M. Robles, J. Unkelbach, B. Vannière, S. Joannin, Late holocene mongolian climate and environment reconstructions from brGDGTs, NPPs and pollen transfer functions for Lake Ayrag: Paleoclimate implications for arid Central Asia. *Quat. Sci. Rev.* **273**, 107235 (2021).
84. D. Ning, E. Zhang, J. Shulmeister, J. Chang, W. Sun, Z. Ni, Holocene mean annual air temperature (MAAT) reconstruction based on branched glycerol dialkyl glycerol tetraethers from Lake Ximenglongtan, southwestern China. *Org. Geochem.* **133**, 65–76 (2019).
85. S. Qian, H. Yang, C. Dong, Y. Wang, J. Wu, H. Pei, X. Dang, J. Lu, S. Zhao, S. Xie, Rapid response of fossil tetraether lipids in lake sediments to seasonal environmental variables in a shallow lake in central China: Implications for the use of tetraether-based proxies. *Org. Geochem.* **128**, 108–121 (2019).
86. M. Woltering, J. P. Werne, J. L. Kish, R. Hicks, J. S. Sinninghe Damsté, S. Schouten, Vertical and temporal variability in concentration and distribution of thaumarchaeotal tetraether lipids in Lake Superior and the implications for the application of the TEX 86 temperature proxy. *Geochim. Cosmochim. Acta* **87**, 136–153 (2012).
87. T. V. Khodzher, V. M. Domysheva, L. M. Sorokovikova, M. V. Sakirko, I. V. Tomberg, Current chemical composition of Lake Baikal water. *Inl. Waters.* **7**, 250–258 (2017).
88. J. Cao, X. Duan, X. Jin, E. Lian, P. Yin, L. Li, G. Jia, Sedimentary core brGDGTs in the East China Sea are mainly produced in situ as evidenced by their similar distributions with brGDGTs derived from intact polar lipids. *Org. Geochem.* **149**, 104095 (2020).
89. C. Zell, J. H. Kim, D. Dorhout, M. Baas, J. S. S. Damsté, Sources and distributions of branched tetraether lipids and crenarchaeol along the Portuguese continental margin: Implications for the BIT index. *Cont. Shelf Res.* **96**, 34–44 (2015).
90. L. Warden, J.-H. Kim, C. Zell, G.-J. Vis, H. De Stigter, J. Bonnin, J. S. S. Damsté, Examining the provenance of branched GDGTs in the Tagus River drainage basin and its outflow into the Atlantic Ocean over the Holocene to determine their usefulness for paleoclimate applications. *Biogeosciences.* **13**, 5719–5738 (2016).
91. Y. Xu, Z. Jia, W. Xiao, J. Fang, Y. Wang, M. Luo, F. Wenzhöfer, A. A. Rowden, R. N. Glud, Glycerol dialkyl glycerol tetraethers in surface sediments from three Pacific trenches: Distribution, source and environmental implications. *Org. Geochem.* **147**, 104079 (2020).

92. M. Ceccopieri, R. S. Carreira, A. L. R. Wagener, J. Hefter, G. Mollenhauer, Branched GDGTs as proxies in surface sediments from the South-Eastern Brazilian continental margin. *Front. Earth Sci.* **7**, 291 (2019).
93. B. D. A. Naafs, G. N. Inglis, Y. Zheng, M. J. Amesbury, H. Biester, R. Bindler, J. Blewett, M. A. Burrows, D. del C. Torres, F. M. Chambers, A. D. Cohen, R. P. Evershed, S. J. Feakins, M. Gałka, A. G.-Sala, L. Gandois, D. M. Gray, P. G. Hatcher, E. N. H. Coronado, P. D. M. Hughes, A. Huguet, M. Könönen, F. L.-Défarge, O. Lähteenoja, M. Lamentowicz, R. Marchant, E. McClymont, X. P.-Pombal, C. Ponton, A. Pourmand, A. M. Rizzuti, L. Rochefort, J. Schellekens, F. De Vleeschouwer, R. D. Pancost, Introducing global peat-specific temperature and pH calibrations based on brGDGT bacterial lipids. *Geochim. Cosmochim. Acta* **208**, 285–301 (2017).
94. C. De Jonge, A. Stadnitskaia, A. Fedotov, J. S. S. Damsté, Impact of riverine suspended particulate matter on the branched glycerol dialkyl glycerol tetraether composition of lakes: The outflow of the Selenga River in Lake Baikal (Russia). *Org. Geochem.* **83-84**, 241–252 (2015).
95. C. V. Freymond, F. Peterse, L. V. Fischer, F. Filip, L. Giosan, T. I. Eglinton, Branched GDGT signals in fluvial sediments of the Danube River basin: Method comparison and longitudinal evolution. *Org. Geochem.* **103**, 88–96 (2017).
96. C. Zell, J.-H. Kim, M. Balsinha, D. Dorhout, C. Fernandes, M. Baas, J. S. Sinninghe Damsté, Transport of branched tetraether lipids from the Tagus River basin to the coastal ocean of the Portuguese margin: Consequences for the interpretation of the MBT′/CBT paleothermometer. *Biogeosciences.* **11**, 5637–5655 (2014).
97. F. M. S. A. Kirkels, C. Ponton, V. Galy, A. J. West, S. J. Feakins, F. Peterse, From Andes to Amazon: Assessing branched tetraether lipids as tracers for soil organic carbon in the madre de Dios river system. *J. Geophys. Res. Biogeo.* **125**, 1–18 (2020).
98. M. Wang, H. Yang, Z. Zheng, L. Tian, Altitudinal climatic index changes in subtropical China indicated from branched glycerol dialkyl glycerol tetraethers proxies. *Chem. Geol.* **541**, 119579 (2020).
99. J. Li, B. D. A. Naafs, R. D. Pancost, H. Yang, D. Liu, S. Xie, Distribution of branched tetraether lipids in ponds from Inner Mongolia, NE China: Insight into the source of brGDGTs. *Org. Geochem.* **112**, 127–136 (2017).
100. Y. Li, S. Zhao, H. Pei, S. Qian, J. Zang, X. Dang, H. Yang, Distribution of glycerol dialkyl glycerol tetraethers in surface soils along an altitudinal transect at cold and humid Mountain Changbai: Implications for the reconstruction of paleoaltimetry and paleoclimate. *Sci. China Earth Sci.* **61**, 925–939 (2018).
101. J. Zang, Y. Lei, H. Yang, Distribution of glycerol ethers in Turpan soils: Implications for use of GDGT-based proxies in hot and dry regions. *Front. Earth Sci.* **12**, 862–876 (2018).
102. M. Wang, Y. Zong, Z. Zheng, M. Man, J. Hu, L. Tian, Utility of brGDGTs as temperature and precipitation proxies in subtropical China. *Sci. Rep.* **8**, 194 (2018).
103. M. Wang, Z. Zheng, Y. Zong, M. Man, L. Tian, Distributions of soil branched glycerol dialkyl glycerol tetraethers from different climate regions of China. *Sci. Rep.* **9**, 1–8 (2019).
104. J. Guo, T. Ma, N. Liu, X. Zhang, H. Hu, W. Ma, Z. Wang, X. Feng, F. Peterse, Soil pH and aridity influence distributions of branched tetraether lipids in grassland soils along an aridity transect. *Org. Geochem.* **164**, 104347 (2021).
105. H. Wang, W. Liu, Soil temperature and brGDGTs along an elevation gradient on the northeastern Tibetan Plateau: A test of soil brGDGTs as a proxy for paleoelevation. *Chem. Geol.* **566**, 120079 (2021).
106. C. Chen, Y. Bai, X. Fang, G. Zhuang, A. Khodzhiev, X. Bai, A. Murodov, Evaluating the potential of soil bacterial tetraether proxies in westerlies dominating western Pamirs, Tajikistan and implications for paleoenvironmental reconstructions. *Chem. Geol.* **559**, 119908 (2021).
107. P. Véquaud, S. Derenne, C. Anquetil, S. Collin, J. Poulenard, P. Sabatier, A. Huguet, Influence of environmental parameters on the distribution of bacterial lipids in soils from the French Alps: Implications for paleo-reconstructions. *Org. Geochem.* **153**, 104194 (2021).

Acknowledgments: We thank S. Kopf for help with coding and figure making, the entire PACEMAP and ILLUME teams, members of the Organic Geochemistry Lab at CU Boulder for fruitful discussions, and all authors who shared additional data. We also thank the editor, G. Bowen, and two reviewers, D. Naafs and J. Werne, for helpful suggestions that greatly improved this manuscript. **Funding:** This work was supported by the National Science Foundation grants OPP-1737712 (to G.H.M. and J.S.), OPP-1836981 (to G.H.M., Á.G., and J.S.), DDRI-1657743 (to G.H.M.); a doctoral grant from the University of Iceland (to Á.G. and J.H.R.); and a project grant from the University of Iceland Research Fund (Á.G.). **Author contributions:** Conceptualization: J.H.R. Methodology: J.H.R. Investigation: J.H.R. Visualization: J.H.R. Supervision: G.H.M., J.S., and Á.G. Writing (original draft): J.H.R. Writing (review and editing): G.H.M., J.S., and Á.G. **Competing interests:** The authors declare that they have no competing interests. **Data and materials availability:** All data needed to evaluate the conclusions in the paper are present in the paper and/or the Supplementary Materials (data file S1) and on the PANGAEA data repository (https://doi.org/10.1594/PANGAEA.940052). There are no restrictions on data availability.

Submitted 11 October 2021
Accepted 1 April 2022
Published 18 May 2022
10.1126/sciadv.abm7625

ScienceAdvances

Near-universal trends in brGDGT lipid distributions in nature

Jonathan H. RabergGifford H. MillerÁslaug GeirsdóttirJulio Sepúlveda

Sci. Adv., 8 (20), eabm7625. • DOI: 10.1126/sciadv.abm7625

Science Advances (ISSN) is published by the American Association for the Advancement of Science. 1200 New York Avenue NW, Washington, DC 20005. The title *Science Advances* is a registered trademark of AAAS.